Article

Cascaded hard X-ray self-seeded free-electron laser at megahertz repetition rate

Check for updates

A list of authors and their affiliations appears at the end of the paper

High-resolution X-ray spectroscopy in the sub-nanosecond to femtosecond time range requires ultrashort X-ray pulses and a spectral X-ray flux considerably larger than that presently available. X-ray free-electron laser (XFEL) radiation from hard X-ray self-seeding (HXRSS) setups has been demonstrated in the past and offers the necessary peak flux properties. So far, these systems could not provide high repetition rates enabling a high average flux. We report the results for a cascaded HXRSS system installed at the European XFEL, currently the only operating high-repetition-rate hard X-ray XFEL facility worldwide. A high repetition rate, combined with HXRSS, allows the generation of millijoule-level pulses in the photon energy range of 6–14 keV with a bandwidth of around 1 eV (corresponding to about 1 mJ eV^{-1} peak spectral density) at the rate of ten trains per second, each train including hundreds of pulses arriving at a megahertz repetition rate. At 2.25 MHz repetition rate and photon energies in the 6–7 keV range, we observed and characterized the heat-load effects on the HXRSS crystals, substantially altering the spectra of subsequent X-ray pulses. We demonstrated that our cascaded self-seeding scheme reduces this detrimental effect to below the detection level. This opens up exciting new possibilities in a wide range of scientific fields employing ultrafast X-ray spectroscopy, scattering and imaging techniques.

Modern hard X-ray free-electron lasers (FELs) provide ultrabright pulses of X-ray radiation[1–4]. In this Article, we discuss a unique combination of a cascaded hard X-ray self-seeding (HXRSS) setup and a multimegahertz-repetition-rate accelerator at the European XFEL[5] that allows delivering thousands of pulses of radiation per second, in 10 Hz bursts, with a spectral density up to 1 mJ eV^{-1} range, thus increasing the average spectral brightness of about two orders of magnitude compared with any other FEL facility. The combination of a high-repetition-rate FEL and an HXRSS setup is currently the only method of enabling new scientific applications requiring a large photon flux in a narrow spectral bandwidth across the hard X-ray spectral region.

Hard X-ray FEL pulses are usually generated by self-amplified spontaneous emission (SASE) starting from shot noise in the electron beam. SASE is characterized by a limited longitudinal coherence[6–8], and it can be challenging to tailor it for experiments where a very narrow bandwidth and high spectral brightness are required[9–12]. Monochromators can passively filter SASE light, but only at the expense of the intensity reaching the sample[8]. Moreover, at a high-repetition-rate facility like the European XFEL, heat-load effects decrease the monochromator transmission even when applying cryo-cooling[13].

Self-seeding[14] is an active frequency-filtering process that overcomes many of these issues by increasing the peak brightness of SASE X-ray pulses and decreasing their spectral bandwidth. In a self-seeding scheme, the SASE FEL radiation generated in the first part of an FEL undulator is monochromatized and subsequently amplified to its final properties in the second part. Compared with seeding techniques based on external laser sources[15–22], which limit the final output to
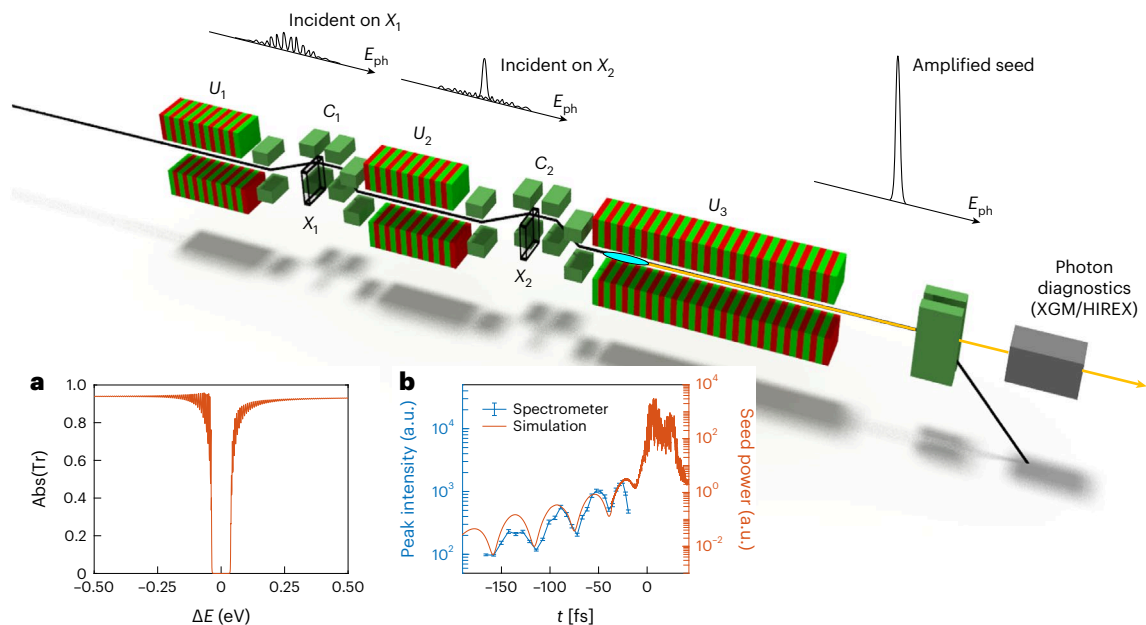
A full list of affiliations appears at the end of the paper. ✉e-mail: gianluca.geloni@xfel.eu

Fig. 1 | Layout of the two-chicane HXRSS setup at the SASE2 undulator of European XFEL. The setup comprises three undulator segments (U_1, U_2 and U_3) and two monochromatization stages (consisting of a combination of a four-dipole chicane C_1 (C_2) and a thin diamond crystal X_1 (X_2)). **a**, A narrow-bandwidth notch is created in the spectrum by means of a thin diamond crystal corresponding to the transmission. **b**, The corresponding intensity profile in the time domain consists of a SASE pulse followed by a trailing wake: red line, calculated (head of the pulse to the right); blue data points, spectrometer peak intensity measured by a delay scan of chicane C_2 at 9 keV with a C*(004) reflection. Data are presented as mean values ± standard error of the mean (s.e.m.); sample size, $n = 100$. The electron bunch (cyan) is overlapped with the seed and amplifies it up to saturation and beyond in U_3. The generated X-ray pulse (yellow) is characterized by the XGM pulse energy monitor and the HIREX single-shot spectrometer (grey), located in the photon beam transport approximately 500 m downstream of the undulator.

nanometre wavelengths, the strength of HXRSS is providing radiation with wavelengths around 0.1 nm and below, enabling atomic-resolution experiments. During the past few years, several self-seeding experiments in the hard X-ray regime have demonstrated the robustness and flexibility of this method[23–25].

However, similar to passive monochromatization at the high repetition rate available at the European XFEL, considerable heat can be deposited in the HXRSS crystal, resulting in intra-train spectral shifts and broadening[26–28]. In this Article, we experimentally study this effect for the first time, finding that below a photon energy of 8 keV, heat-load effects become important. To cope with these detrimental effects, a cascaded two-chicane HXRSS system has been designed and installed at the European XFEL. Here we demonstrate that the use of a cascaded HXRSS setup with two chicanes reduces crystal heat-load effects to below the detection level. Our HXRSS setup provides pulses with a spectral density up to 1 mJ eV^{-1} range. The unique combination with a multimegahertz-repetition-rate accelerator results in about two orders of magnitude increase in average brightness compared with any other HXRSS setup worldwide.

These results open up exciting possibilities in a wide range of scientific fields. An important class of applications is constituted by Mössbauer spectroscopy at X-ray FELs[29,30], including—in particular—nuclear resonances with femto-electronvolt bandwidth for extreme metrology applications with ultraprecise atomic clocks and investigations of condensed-matter dynamics and phase transitions, an important case being the resonant excitation[31] of the nuclear clock isomer ^{45}Sc. Such applications require higher spectral brightness (peak and average) than available today at X-ray FELs with or without a monochromator (even at high repetition rates).

Another promising application is constituted by inelastic X-ray scattering, which is also in need of large spectral density[32,33]. It is often preferable to perform inelastic X-ray scattering at lower photon

Table 1 | Average beam properties for SASE and cascaded HXRSS at three photon energies

	Photon energy		
	7.5 keV (*)	**9.0 keV**	**13.0 keV**
Electron-beam energy	14.0 GeV	14.0 GeV	16.5 GeV
SASE mode			
Pulse energy	(1.5±0.3) mJ	(2.2±0.2) mJ	(2.2±0.4) mJ
Bandwidth (FWHM)	10 eV	20 eV	19 eV
Spectral density	110 μJ eV^{-1}	100 μJ eV^{-1}	90 μJ eV^{-1}
HXRSS mode			
Total pulse energy	(1.1±0.4) mJ	(1.2±0.3) mJ	(0.8±0.3) mJ
SASE contribution	0.1 mJ	0.4 mJ	0.3 mJ
Bandwidth (FWHM)	1.3 eV	0.8 eV	0.7 eV
Spectral density	600 μJ eV^{-1}	1,000 μJ eV^{-1}	700 μJ eV^{-1}

Only the first pulses in each pulse train were considered here. The asterisk indicates operation with two chicanes. The uncertainties reported are r.m.s. jitters calculated on the basis of the integrated spectrometer data for a sample size of 1,000 pulses.

energies, for instance, below 8 keV. For example, the High Energy Density scientific instrument at European XFEL operates an inelastic X-ray scattering spectrometer using Si(533), Si(333), Si(444) or Si(555) reflection. Working in the backscattering geometry, the angular acceptance is optimized and still maintains good energy resolution. The photon energies for the backscattering of these reflections are in the range around and below 8 keV.

The third important application is constituted by wide-angle X-ray photon correlation spectroscopy (XPCS)[34,35]. Since speckles
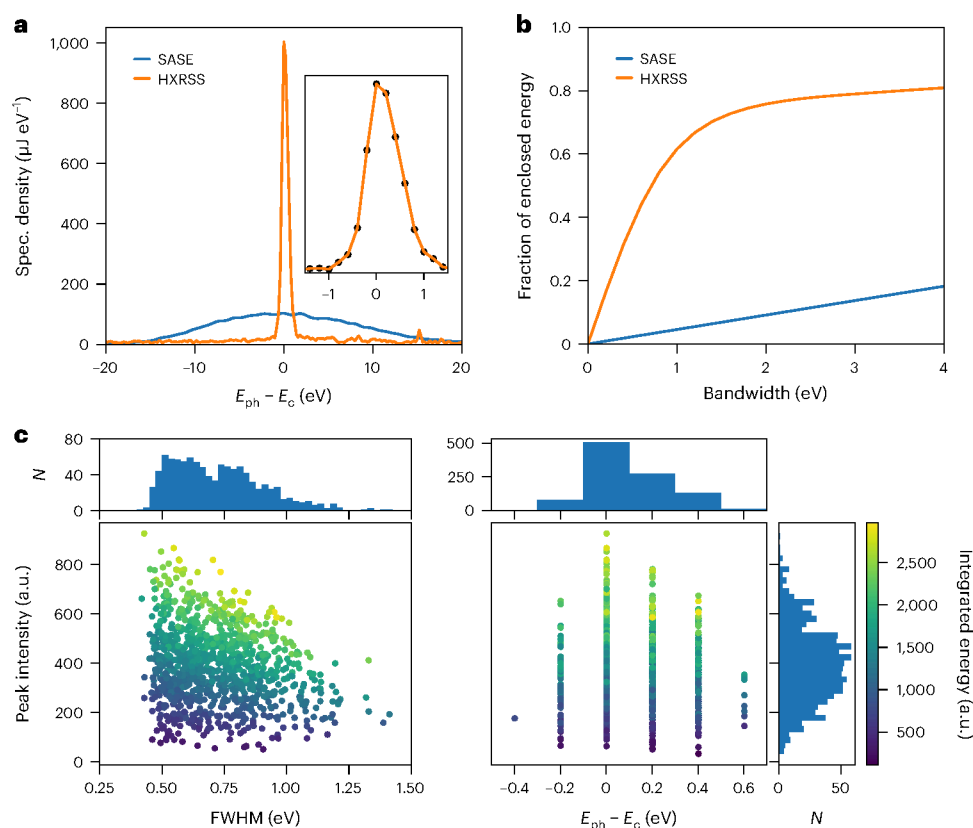
Fig. 2 | HXRSS performance achieved at 9 keV. a, Comparison of the best seeded (HXRSS) pulse (central energy E_c = 9,009.0 eV; average energy, 1.2 mJ; 400 μJ background; FWHM bandwidth, 0.8 eV) with typical SASE at the European XFEL (pulse energy, 2.2 mJ; FWHM bandwidth, 20.0 eV). The seeded pulse reaches 1 mJ eV^{-1} spectral density, obtained by delaying the electron bunches by 45 fs. **b**, Enclosed pulse energy fraction against bandwidth for HXRSS and plain SASE. **c**, Statistics for the HXRSS working point. The central-energy r.m.s. jitter was 0.17 eV, the peak-intensity r.m.s. jitter was 40%, mean of the FWHM bandwidth was 0.72 eV and FWHM-bandwidth r.m.s. jitter was 0.18 eV.

and contrast from coherent scattering signals become smaller at higher photon energy, XPCS experiments are best performed at as low a photon energy as possible. The wide-angle scattering geometry also requires a much better defined bandwidth than for coherent small-angle X-ray scattering, typically on the order of 10^{-4}. Many synchrotron beamlines operate such wide-angle XPCS experiments around a photon energy of 6–7 keV. We, therefore, foresee exciting HXRSS wide-angle megahertz-range XPCS applications at the European XFEL, similar to the recent small-angle X-ray scattering–XPCS work done at 9 keV (ref. 36) at the Materials Imaging and Dynamics instrument.

Cascaded HXRSS system

The European XFEL consists of two hard X-ray undulators, namely, SASE1 and SASE2, and one soft X-ray undulator, namely, SASE3 (ref. 5). The cascaded HXRSS system is integrated into the SASE2 undulator (Fig. 1 and Supplementary Section 1). This system can be used in different modes, including the SASE mode (no chicane is used), one-chicane mode (only one of the two chicanes is used) and two-chicane mode (both chicanes are used). For the two-chicane mode, the operation is set up in three subsequent steps, relying on the transmissive monochromator concept[37]. First, a notch is introduced in the SASE spectrum generated by the first part of undulator U_1, by means of transmission through a thin diamond crystal X_1, oriented to satisfy Bragg's condition (Fig. 1a and Supplementary Section 3). In the time domain, this frequency notch corresponds to a trailing wake of monochromatic radiation—the seed—delayed with respect to the main SASE pulse (Fig. 1b). Second, the electron bunch is delayed by a magnetic chicane C_1 (Supplementary Section 2) and overlapped with the seed.

Since the longitudinal dispersion of the chicane (corresponding to a delay of a few tens of femtoseconds) is large enough to wash out the SASE microbunching and the power in the seed is much larger than the equivalent SASE shot-noise level, the seed can be amplified in a second undulator part U_2. These first two steps are common for all the HXRSS systems based on the transmissive monochromator concept. However, unique to our setup, in the third step, the seeded pulse is incident on the second crystal X_2 at the same angle as for X_1 to further monochromatize the seed pulse and generate another seed. This is then overlapped again with the electron bunch after the second magnetic chicane C_2 and further amplified in the last undulator part U_3. Amplification of the pulse beyond saturation is enabled by a nonlinear variation in the undulator strength as a function of position. This process, known as tapering, maintains the resonance between electrons and the seeded pulse, and is enabled by the availability of a long hard X-ray undulator with a variable magnetic gap (a total of 35 undulator segments corresponding to 175 m of magnetic length).

Operation with a cascaded HXRSS system leads to clear advantages for X-ray FELs like the European XFEL[5], the first hard X-ray facility worldwide driven by a superconducting linear accelerator and operating at a megahertz repetition rate. In contrast to X-ray FELs driven by normal conducting linear accelerators, typically delivering about hundred pulses per second, the European XFEL provides ten bursts of X-ray pulses every second, each burst typically consisting of several hundred pulses (up to 2,700) at an intra-train repetition rate of 4.5 MHz, or subharmonics thereof. Seeded operation at these repetition rates increases the average brightness of the X-ray pulses of up to two orders of magnitude, but at photon energies lower than about
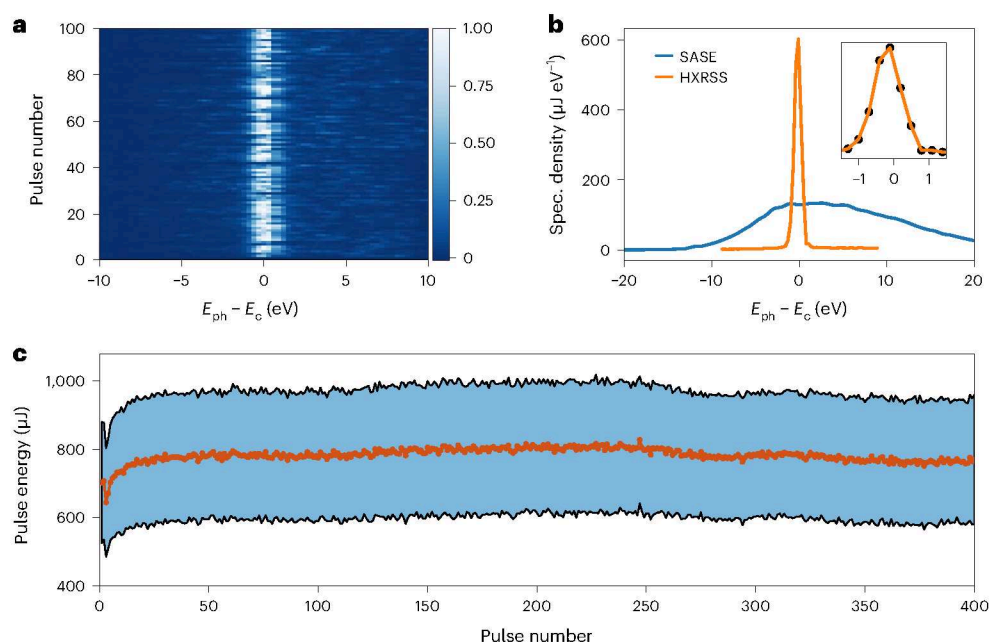
Fig. 3 | HXRSS performance during user delivery at a high repetition rate.
a, Spectra of every fourth pulse within a single train at 2.25 MHz at E_c = 8,996 eV.
There is neither a shift in the central photon energy nor a change in the spectrum
along the train, indicating the absence of heat-load effects. **b**, Comparison
between seeded and SASE pulses, averaged over 1,000 pulses, with a single pulse
per train, for an overall value of ten pulses per second. The spectral density in
the seeded mode increased by a factor of 4.5. The central energy of the seeded

signal was E_c with a single-shot FWHM bandwidth of about 0.9 eV. The SASE
central energy was slightly shifted to E_{c2} = 8,999.0 eV with an FWHM bandwidth of
about 19.2 eV. **c**, Pulse energy as a function of pulse number after orbit correction
according to the centre of the pulse train in the self-seeding configuration. The
red dots are average values; the half-width of the coloured band indicates the
standard deviation computed from 1,000 trains.

8 keV, it also generates a considerable heat load on the HXRSS crystal,
leading to intra-train spectral shifts and broadening[26–28]. In this Article,
we report the first experimental results on how cascaded HXRSS can
be used to compensate these detrimental effects. The working princi-
ple relies on the fact that although the FEL pulse incident on the first
crystal X_1 is only SASE, the FEL pulse incident on X_2 is seeded. Therefore,
for fixed and equal incident energies on X_1 and X_2, the spectrum of the
signal incident on X_2 has a higher spectral density (Fig. 1). Consequently,
the final seed signal in U_3 is larger in the case of a cascaded HXRSS mono-
chromator[26]. In other words, cascading increases the signal-to-noise
ratio between the incident seed and SASE background. We use this
increased ratio to decrease the incident pulse energy on the crystals
compared with what would be needed with a single HXRSS setup. This
eases the heat load from FEL radiation, which is dominant at low photon
energies, over the contribution of spontaneous radiation[26]. As a result,
cascading two HXRSS setups reduces the heat load and enables HXRSS
at megahertz repetition rates.

For photon energies above 8 keV, with an incident pulse energy
below 50 μJ, the heat-load impact on the crystal was found to be
negligible in our experiments. Therefore, at these photon energies,
the cascaded HXRSS system can also be operated in the single-chicane
mode. In this case, the second chicane (C_2) is chosen to obtain a
higher incident pulse energy on the crystal and to simplify the setup
procedure.

Table 1 summarizes the performance and main achievements at
three photon energies for SASE and cascaded HXRSS. Only the first
pulses in each pulse train were considered in this table. At the European
XFEL, the seeded mode is requested by users at a high repetition rate
at different photon energies currently ranging from 6 to 14 keV. The
seeded beam is delivered to users on a regular basis with considerably
increased spectral density compared with SASE.

In the following sections, we will report on the best performance
in terms of spectral density, on the delivery of high-repetition-rate

pulses at 9.0 keV and on the impact of heat load at low photon ener-
gies (6.0 and 7.5 keV), which can be minimized by cascaded seeding
employing both chicanes (Supplementary Section 9 provides more
details concerning the 13.0 keV case). In all of the following illustrations,
the electron bunch charge used was 250 pC and the electron-beam
energy was 14 GeV.

High spectral density
The highest spectral density achieved at the European XFEL in the
single-chicane (C_2) mode was obtained by operating with a single
bunch per train, that is, at a rate of 10 Hz, at around 9 keV photon energy.
Figure 2a shows the seeded performance, with an average pulse energy
of 1.2 mJ and a full-width at half-maximum (FWHM) of 0.8 eV, compared
with the SASE performance of about 2.2 mJ and FWHM of 20.0 eV. Both
spectra are averaged over 1,000 pulses. The background was measured
by extracting the crystal and amounted to 400 μJ (Supplementary Sec-
tion 5). Here the C*(004) reflection was used and the optimum chicane
delay was found to be 45 fs.

The seeded pulses reach an average of 1 mJ eV⁻¹ peak spectral
density, which is the maximum of the single-shot averaged spectrum
shown in Fig. 2a, and hence exceed SASE by a factor of ten. Figure 2b
shows the photon fraction within a given bandwidth as a function of
that bandwidth. More than 50% of the seeded pulse is enclosed within
±0.5 eV from the central photon energy, compared with less than 2%
of the SASE pulse (Supplementary Section 4 discusses the impact of
the electron-beam phase-space characteristics on the HXRSS perfor-
mance). Figure 2c shows a statistical analysis of the seeded data. The
peak intensity in each spectrum is represented in a scatter plot, the
lowest peaks corresponding to the lowest total pulse energy. Here
the FEL pulses were recorded after saturation and undulator tapering
was applied. The resolution of the spectrometer was 0.2 eV per pixel
(a bent silicon crystal was used as the dispersive element; Methods)
and approximately 500 pulses out of the ensemble (1,000 pulses) was
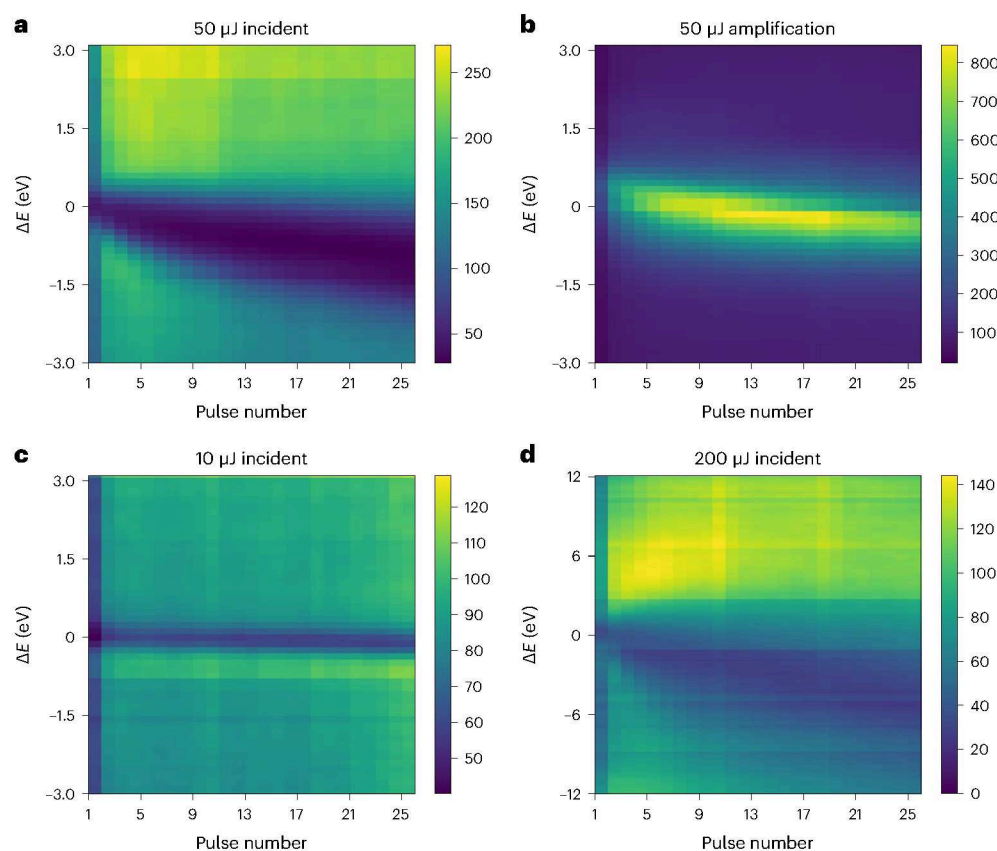
Fig. 4 | Heat-load effects at 6 keV photon energy. a,b, Colour-coded spectra as a function of position down the pulse train (one pulse spectrum in four was recorded by the spectrometer) in the case of 50 μJ average SASE pulse energy incident on the self-seeding crystal C_2, showing the evolution of the notch down the train (**a**) and the amplified self-seeded signal (**b**). **c,d,** Evolution of the notch down the train in the cases of 10 μJ (**c**) and 200 μJ (**d**) average SASE pulse energy incident on the self-seeding crystal C_2.

within one pixel. The central-energy r.m.s. jitter was 0.17 eV and the FWHM-bandwidth r.m.s. jitter was 0.18 eV. Note that there are almost no pulses with an FWHM bandwidth narrower than 0.5 eV. This is not limited by the spectrometer resolution, which is 0.2 eV. The peak-intensity r.m.s. jitter was about 40% (Supplementary Section 7).

High repetition rate

The high-repetition-rate performance of HXRSS at a central photon energy of E_c = 8,996 eV is reported in Fig. 3. The data were taken in a different operation mode for users, providing 400 pulses per train at 2.25 MHz that amount to 4,000 pulses per second. As discussed earlier, the setup relies on the second chicane (C_2) only, and operates with the symmetric C*(004) reflection. However, the optimum chicane delay was found to be 19 fs, much shorter than in the previous section, due to an effectively shorter bunch length of the electron beam.

The spectral analysis made on a single train (Fig. 3a) showed neither deviation from the central photon energy along a train nor changes in the spectral bandwidth. The FWHM, averaged over 100 pulses, is around 1.3 eV. For Fig. 3a,b, we estimated a spectrometer resolution of 0.3 eV per pixel (a bent diamond crystal was used as the dispersive element; Methods). Even for the case here, this confirmed that there was no visible degradation in the seeding quality and stability caused by the heat load of the crystal. Therefore, the pulse energy could be taken as the relevant figure of merit and the X-ray gas monitor (XGM) detector was used as a diagnostics device throughout the run[38,39]. Figure 3c shows the distribution of pulse energies recorded by the XGM as a function of the intra-train pulse number after orbit correction. The first pulses in the train are systematically

underperforming due to a slightly different orbit, ascribed to imperfect correction (Supplementary Section 6). The non-perfect orbit correction also resulted in a reduced average peak spectral density (Fig. 3b) compared with the best performance reported in Fig. 2a. HXRSS still increased the peak spectral density by about 4.5 times compared with the best SASE performance reached on the same day (Fig. 3b). On average, the seeded pulse carried about 800 μJ energy, compared with about 3 mJ for the SASE case. The SASE background was estimated by extracting the crystal and amounted to less than 250 μJ.

Mitigation of heat load by cascaded HXRSS

At lower photon energies, namely, 6.0 and 7.5 keV, the energy absorbed by the seeding crystal increases, and heat-load effects in the single-chicane setup become measurable and detrimental. For a 100 μm crystal, we estimate[40] the absorbed FEL pulse energy at 6.0 keV to be about 31% of the total and at 7.5 keV, to be about 17%; at 9.0 keV, it drops to 10%. For an incident pulse energy on the crystal of 40 μJ, this results in 12.4, 6.8 and 4.0 μJ of absorbed energy, respectively. It should be noted that the HXRSS system at the European XFEL does not rely on cooling of the crystals. As discussed in another work[26], the heat does not have time to diffuse to the crystal edges between pulses in a pulse train, leading to a situation where steady state cannot be reached.

The performance of HXRSS at 6 keV was studied by seeding with the second chicane C_2 for different amounts of incident SASE energies on the crystal. During this experiment, the chicane delay was 30 fs and the crystal reflection used was C*(111). The results are illustrated in Fig. 4, where we show the colour-coded spectra for different pulses along the train averaged over 900 trains. Here ΔE is defined as the
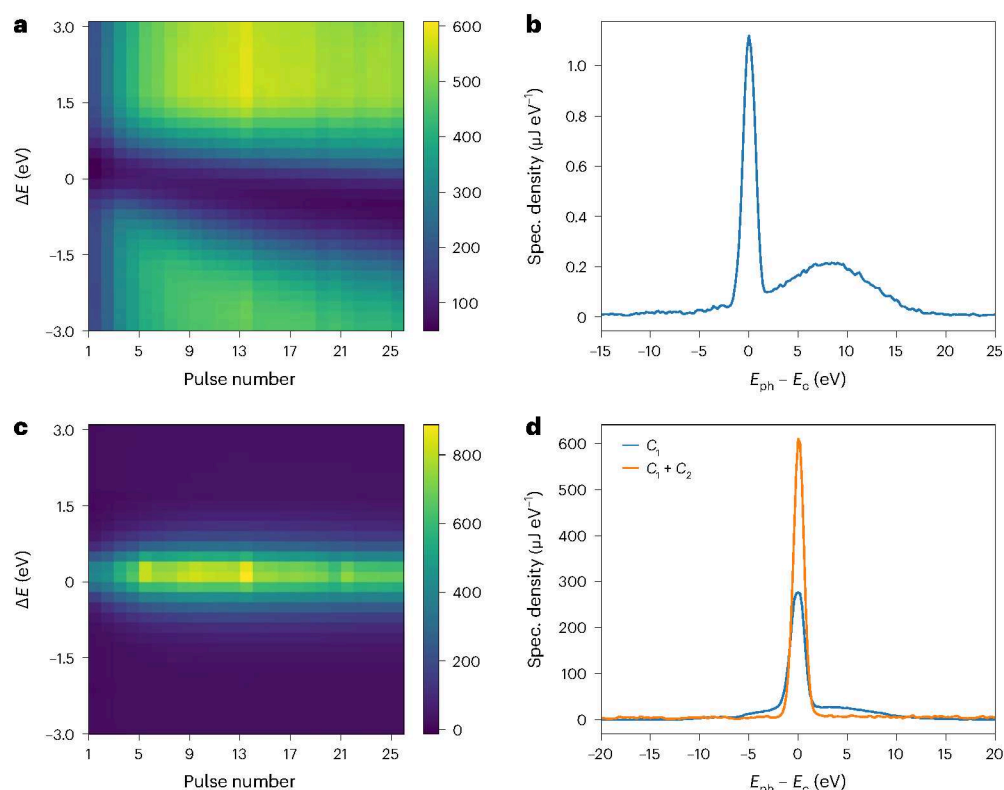
Fig. 5 | Performance of different HXRSS configurations at 7.5 keV. a, Evolution of the notch down the train with an incident SASE energy of 40 μJ on the second crystal X_2. **b**, Spectrum of the incident pulse at the second crystal X_2, averaged over 1,000 pulses. The incident energy is estimated in the several microjoules level. The self-seeded spectral peak at $E_c = 7,440.1$ eV incident on X_2 has an FWHM bandwidth of 1.2 eV and is about five times higher than the SASE peak. **c**, Colour-coded average spectrum, as a function of the position down trains of 100 pulses, simultaneously seeding with C_1 and C_2 (one event in four was recorded by the spectrometer). **d**, Comparison of the best seeded performances with the first chicane C_1 (blue), and with the first and second chicanes $C_1 + C_2$ (simultaneous seeding) (orange). Both spectra are averaged over 1,000 pulses.

photon energy difference with respect to the central energy. The accelerator was running at a repetition rate of 2.25 MHz with 100 pulses per train. However, the high-resolution hard X-ray (HIREX) spectrometer was only recording one spectrum out of every four pulses. Therefore, for a total of 100 pulses, only 25 pulses are shown on the horizontal axis (Fig. 4). The study was performed with the undulator part after C_2 (responsible for amplification) open (Fig. 4a,c,d, where the effect of the notch on the spectrum is visible) and closed (Fig. 4b, where the seeded signal after amplification is shown).

In the case of an average incident SASE energy of 50 μJ, a change in the shape of the spectral notch along the train can be observed (Fig. 4a): within 100 pulses, it becomes wider, with a central shift of about 0.8 eV. The width of the spectral notch increases from 0.7 to 1.8 eV, which is comparable with the HXRSS bandwidth, namely, 1.0 eV FWHM. The corresponding amplified signal is shown in Fig. 4b: the effect of the 0.8 eV shift in the notch is reflected in an analogous shift in the spectral peak of the self-seeded signal. When incident with about 10 μJ (Fig. 4c), there are no heat-load effects on the notch. However, the incident energy is too small for signal amplification. Finally, in the case of about 200 μJ incident average SASE energy (Fig. 4d), one can observe a much stronger influence of the heat load, and the seed could not be amplified anymore. This is attributed to a combined effect of poor seed signal due to the widening notch bandwidth and a spoiled electron beam.

Similar studies have been performed at 7.5 keV, using the same crystal reflection C*(111). In this case, the optimal incident SASE energy level was found to be 35–40 μJ, as recorded by the XGM (Supplementary Section 8). Once the optimal incident SASE FEL pulse energy was found, working at 2.25 MHz repetition rate but with 400 pulses per train, we observed a change in the notch shape, and a shift in the central energy of 1.6 eV, qualitatively similar to the 6.0 keV case (Fig. 5a).

To mitigate the heat-load effect on the crystal, simultaneously seeding with both HXRSS systems ($C_1 + C_2$) was performed, with delays set to 24 and 16 fs, respectively. In the case of $C_1 + C_2$, the energy level incident on the first and second crystals was estimated to be in the few microjoules level. However, since it was already seeded by the first crystal (Fig. 5b), a higher signal-to-noise ratio could be achieved, the signal being the incident seed and the noise being the incident SASE. Note that in Fig. 5b, both SASE background and seed signal from the first chicane are visible at the same energy (7.5 keV in this case). If the first crystal is removed, the second crystal would be hit by a small and relatively broadband SASE pulse around the main peak (Fig. 5b). By inserting the first crystal, instead, we seed with the peak at $E_{ph} = E_c$. This peak is about a factor of five higher than the SASE maximum, and this factor of five is the signal-to-noise increase in the incident peak spectral density. The higher spectral density available for the generation of the seed signal after the second chicane resulted in a spectrum with about 0.9 eV FWHM bandwidth, and with central energy changes along the train smaller than the spectrometer resolution (Fig. 5c).

Different performances obtained for seeding with C_1 only, or with $C_1 + C_2$, are summarized in Fig. 5d. Data refer to a single pulse in the train, averaged over 1,000 trains, and correspond to the best performances achieved (on different days). In the case of seeding with C_1 only, the central photon energy E_c is 7,440.7 eV with 270 μJ eV^{-1} spectral density and 0.8 eV FWHM bandwidth. Note the presence of side bands around the main peak, which we ascribe to an insufficient seeding power.

Using both first and second chicanes $C_1 + C_2$, we were able to seed at $E_c = 7{,}440.1$ eV, with 600 µJ eV^{-1} spectral density and 0.8 eV FWHM bandwidth, without any heat-load effects (the data in Fig. 5c are with the same level of incident energy) and no visible side bands.

Discussion and conclusion

Cascaded hard X-ray self-seeding has been demonstrated at the European XFEL in the burst-mode operation at 2.25 MHz, with up to 4,000 pulses per second. The photon energy range currently explored spans from 6 to 14 keV. At low photon energies of 6.0 and 7.5 keV, heat load on the crystal was confirmed for the first time, to the best of our knowledge, to affect the spectral properties of radiation at a megahertz repetition rate, by a shift in the central lasing wavelength along the pulse train. The cascaded setup with two chicanes can be used to mitigate heat-load effects by increasing the spectral density of the seed, at the price of a slightly more complicated tuning and energy scan procedure. The latter, however, is straightforward to be automated.

For photon energies above 8 keV, the heat-load effect is proven to be negligible; therefore, one can use a single chicane (C_2) to obtain a higher incident pulse energy on the crystal and to simplify the setup procedure. With this setup, we have achieved a maximum spectral density of about 1 mJ eV^{-1} at 9 keV, corresponding to about 4 W eV^{-1} of X-ray average power density with 4,000 bunches per second. At 13 keV, we observed a factor of eight increase in the spectral density with respect to SASE (Table 1) in terms of spectral brightness. A mildly amplified seeded signal was also observed at 18 keV, which we believe can be further optimized by the investigation of machine settings. There is no sharp theoretical limit for HXRSS towards higher photon energies. However, the equivalent shot-noise SASE level becomes larger with increasing photon energy, and the gain length becomes longer, leading to an effective decrease in the seed and undulator length available for amplification. We plan to study the amplification at higher photon energies in the future and to compare with alternative methods for reaching higher photon energies that are currently under investigation, for example, by relying on harmonics of the fundamental wavelength.

The HXRSS system at the European XFEL is in operation and highly demanded by users. In the first year, it already enabled more than ten different user groups to perform experiments (that is, about 35% of the scheduled delivery time). Future work on the HXRSS setup will, therefore, include developments for fast setup tuning and routine operation and—at the same time—performance improvements in terms of spectral reach, stability and spectral density, as well as advanced techniques (for example, two-colour seeding[41] and harmonics-based methods).

Online content

Any methods, additional references, Nature Portfolio reporting summaries, source data, extended data, supplementary information, acknowledgements, peer review information; details of author contributions and competing interests; and statements of data and code availability are available at https://doi.org/10.1038/s41566-023-01305-x.

References

1. Emma, P. et al. First lasing and operation of an ångstrom-wavelength free-electron laser. *Nat. Photon.* **4**, 641–647 (2010).
2. Ishikawa, T. et al. A compact X-ray free-electron laser emitting in the sub-ångström region. *Nat. Photon.* **6**, 540–544 (2012).
3. Kang, H.-S. et al. Hard X-ray free-electron laser with femtosecond-scale timing jitter. *Nat. Photon.* **11**, 708–713 (2017).
4. Prat, E. et al. A compact and cost-effective hard X-ray free-electron laser driven by a high-brightness and low-energy electron beam. *Nat. Photon.* **14**, 748–754 (2020).
5. Decking, W. et al. A MHz-repetition-rate hard X-ray free-electron laser driven by a superconducting linear accelerator. *Nat. Photon.* **14**, 391–397 (2020).
6. Kondratenko, A. & Saldin, E. Generation of coherent radiation by a relativistic electron beam in an ondulator. *Part. Accel.* **10**, 207–216 (1980).
7. Bonifacio, R. & Casagrande, F. Instabilities and quantum initiation in the free-electron laser. *Opt. Commun.* **50**, 251–255 (1984).
8. Lee, S. et al. High wavevector temporal speckle correlations at the Linac Coherent Light Source. *Opt. Express* **20**, 9790–9800 (2012).
9. Hruszkewycz, S. O. et al. High contrast X-ray speckle from atomic-scale order in liquids and glasses. *Phys. Rev. Lett.* **109**, 185502 (2012).
10. Van Thor, J. J. & Madsen, A. A split-beam probe-pump-probe scheme for femtosecond time resolved protein X-ray crystallography. *Struct. Dyn.* **2**, 014102 (2015).
11. Lu, W. et al. Development of a hard X-ray split-and-delay line and performance simulations for two-color pump-probe experiments at the European XFEL. *Rev. Sci. Instrum.* **89**, 063121 (2018).
12. Roseker, W. et al. Towards ultrafast dynamics with split-pulse X-ray photon correlation spectroscopy at free electron laser sources. *Nat. Commun.* **9**, 1704 (2018).
13. Petrov, I. et al. Performance of a cryo-cooled crystal monochromator illuminated by hard X-rays with MHz repetition rate at the European X-ray Free-Electron Laser. *Opt. Express* **30**, 4978–4987 (2022).
14. Feldhaus, J., Saldin, E., Schneider, J., Schneidmiller, E. & Yurkov, M. Possible application of X-ray optical elements for reducing the spectral bandwidth of an X-ray SASE FEL. *Opt. Commun.* **140**, 341–352 (1997).
15. Yu, L. H. Generation of intense UV radiation by subharmonically seeded single-pass free-electron lasers. *Phys. Rev. A* **44**, 5178–5193 (1991).
16. Stupakov, G. Using the beam-echo effect for generation of short-wavelength radiation. *Phys. Rev. Lett.* **102**, 074801 (2009).
17. Deng, H. & Feng, C. Using off-resonance laser modulation for beam-energy-spread cooling in generation of short-wavelength radiation. *Phys. Rev. Lett.* **111**, 084801 (2013).
18. Hemsing, E., Stupakov, G., Xiang, D. & Zholents, A. Beam by design: laser manipulation of electrons in modern accelerators. *Rev. Mod. Phys.* **86**, 897 (2014).
19. Allaria, E. et al. Two-stage seeded soft-X-ray free-electron laser. *Nat. Photon.* **7**, 913–918 (2013).
20. Ackermann, S. et al. Generation of coherent 19- and 38-nm radiation at a free-electron laser directly seeded at 38 nm. *Phys. Rev. Lett.* **111**, 114801 (2013).
21. Ribič, P. R. et al. Coherent soft X-ray pulses from an echo-enabled harmonic generation free-electron laser. *Nat. Photon.* **13**, 555–561 (2019).
22. Yan, J. et al. Self-amplification of coherent energy modulation in seeded free-electron lasers. *Phys. Rev. Lett.* **126**, 084801 (2021).
23. Amann, J. et al. Demonstration of self-seeding in a hard-X-ray free-electron laser. *Nat. Photon.* **6**, 693–698 (2012).
24. Inoue, I. et al. Generation of narrow-band X-ray free-electron laser via reflection self-seeding. *Nat. Photon.* **13**, 319–322 (2019).
25. Nam, I. et al. High-brightness self-seeded X-ray free-electron laser covering the 3.5 keV to 14.6 keV range. *Nat. Photon.* **15**, 435–441 (2021).
26. Liu, S. et al. Preparing for high-repetition rate hard X-ray self-seeding at the European X-ray Free Electron Laser: challenges and opportunities. *Phys. Rev. Accel. Beams* **22**, 060704 (2019).
27. Qu, Z., Ma, Y., Zhou, G. & Wu, J. Thermal loading on self-seeding monochromators in X-ray free electron lasers. *Nucl. Instrum. Methods Phys. Res. A* **969**, 163936 (2020).
28. Qu, Z., Ma, Y., Zhou, G. & Wu, J. Numerical characterization of quasi-steady thermal load for thin crystal at cryogenic temperature with nondiffusive heat transfer. *J. Appl. Phys.* **130**, 144503 (2021).

29. Röhlsberger, R. *Nuclear Condensed Matter Physics with Synchrotron Radiation: Basic Principles, Methodology and Applications* Vol. 208 (Springer Science & Business Media, 2004).

30. Chumakov, A. I. et al. Superradiance of an ensemble of nuclei excited by a free electron laser. *Nat. Phys.* **14**, 261–264 (2018).

31. Shvyd'ko, Y. et al. Resonant X-ray excitation of the nuclear clock isomer ⁴⁵Sc. *Nature* (2023); https://doi.org/10.1038/s41586-023-06491-w

32. Burkel, E. *Inelastic Scattering of X-Rays with Very High Energy Resolution* Vol. 125 (Springer, 2006).

33. Chubar, O. et al. Ultra-high-resolution inelastic X-ray scattering at high-repetition-rate self-seeded X-ray free-electron lasers. *J. Synchrotron Rad.* **23**, 410–424 (2016).

34. Grübel, G., Stephenson, G., Gutt, C., Sinn, H. & Tschentscher, T. XPCS at the European X-ray free electron laser facility. *Nucl. Instrum. Methods Phys. Res. A* **262**, 357–367 (2007).

35. Lehmkühler, F. et al. Emergence of anomalous dynamics in soft matter probed at the European XFEL. *Proc. Natl Acad. Sci. USA* **117**, 24110–24116 (2020).

36. Reiser, M. et al. Resolving molecular diffusion and aggregation of antibody proteins with megahertz X-ray free-electron laser pulses. *Nat. Commun.* **13**, 5528 (2022).

37. Geloni, G., Kocharyan, V. & Saldin, E. A novel self-seeding scheme for hard X-ray FELs. *J. Mod. Opt.* **58**, 1391–1403 (2011).

38. Maltezopoulos, T. et al. Operation of X-ray gas monitors at the European XFEL. *J. Synchrotron Rad.* **26**, 1045–1051 (2019).

39. Sorokin, A. A. et al. An X-ray gas monitor for free-electron lasers. *J. Synchrotron Rad.* **26**, 1092–1100 (2019).

40. Henke, B., Gullikson, E. & Davis, J. X-ray interactions: photoabsorption, scattering, transmission, and reflection at E=50-30,000 eV, Z=1-92. *At. Data Nucl. Data Tables* **54**, 181–342 (1993).

41. Serkez, S. et al. Generating trains of attosecond pulses with a free-electron laser. In *Proc. 39th International Free-Electron Laser Conference* 692–694 (JACoW Publishing, 2019).

Shan Liu[1], **Christian Grech**[1], **Marc Guetg**[1], **Suren Karabekyan**[2], **Vitali Kocharyan**[1], **Naresh Kujala**[2], **Christoph Lechner**[2], **Tianyun Long**[1,3], **Najmeh Mirian**[1], **Weilun Qin**[1], **Svitozar Serkez**[2], **Sergey Tomin**[1], **Jiawei Yan**[2], **Suren Abeghyan**[2], **Jayson Anton**[4], **Vladimir Blank**[5], **Ulrike Boesenberg**[2], **Frank Brinker**[1], **Ye Chen**[1], **Winfried Decking**[1], **Xiaohao Dong**[2,6], **Steve Kearney**[4], **Daniele La Civita**[2], **Anders Madsen**[2], **Theophilos Maltezopoulos**[2], **Angel Rodriguez-Fernandez**[2], **Evgeni Saldin**[1], **Liubov Samoylova**[2], **Matthias Scholz**[1], **Harald Sinn**[2], **Vivien Sleziona**[2,7], **Deming Shu**[4], **Takanori Tanikawa**[2,8], **Sergey Terentiev**[5], **Andrei Trebushinin**[2], **Thomas Tschentscher**[2], **Maurizio Vannoni**[2], **Torsten Wohlenberg**[1], **Mikhail Yakopov**[2] & **Gianluca Geloni**[2] ✉

[1]Deutsches Elektronen-Synchrotron DESY, Hamburg, Germany. [2]European XFEL, Schenefeld, Germany. [3]Peking University, Beijing, China. [4]Argonne National Laboratory, Argonne, USA. [5]Technological Institute for Superhard and Novel Carbon Materials, Troitsk, Russian Federation. [6]Present address: Shanghai Synchrotron Radiation Facility, Shanghai, China. [7]Present address: Fritz-Haber Institute of the Max Planck Society, Berlin, Germany. [8]Present address: The High Energy Accelerator Research Organization KEK, Oho, Tsukuba, Japan. ✉e-mail: gianluca.geloni@xfel.eu

Methods

Photon diagnostics

The X-ray spectra shown in this Article were collected with the high-resolution hard X-ray single-shot spectrometer II (HIREX-II spectrometer) installed in the XTD6 tunnel of the SASE2 undulator. HIREX-II is identical to the HIREX spectrometer installed at the SASE1 undulator[42], with the difference that it does not include gratings that can be used as a beamsplitter. Thus, the spectrometer crystal has to be placed in the direct beam to collect the energy spectra. For the spectral measurements at a high repetition rate (that is, in the megahertz mode with multiple pulses per train; Fig. 3), a bent diamond (110)-cut crystal using the C*(220) reflection was employed as the dispersive element and a Gotthard detector[43] was used. This has a resolution of 0.3 eV per pixel. However, in the case of the data shown in Fig. 2, a bent silicon (110)-cut crystal using the Si(440) reflection as the dispersive element was exploited to obtain a higher resolution of 0.2 eV per pixel. This is only possible at low repetition rates (that is, in the 10 Hz mode with a single pulse per train), because silicon crystals are more prone to radiation damage compared with diamond crystals.

XGMs parasitically measure absolutely calibrated single-shot pulse energies and average beam positions[38,39]. The basic mechanism of the XGM is the photoionization of rare gas atoms. In the present study, the XGM was operated with xenon. The uncertainty in the pulse energy measurement is 7–10% and the beam position is measured with an uncertainty of ±10 μm. Note that when the energy goes below the XGM accuracy level (at the standard SASE optimized XGM setup, that is, <20 μJ), the intensity was estimated by cross-calibrating XGM and HIREX spectrometer readings at higher pulse energies.

Data availability

The datasets generated during and/or analysed during the current study together with the scripts used to generate the figures are available from the corresponding author on reasonable request.

References

42. Kujala, N. et al. Hard X-ray single-shot spectrometer at the European X-ray Free-Electron Laser. *Rev. Sci. Instrum.* **91**, 103101 (2020).
43. Mozzanica, A. et al. The GOTTHARD charge integrating readout detector: design and characterization. *J. Instrum.* **7**, C01019 (2012).

Acknowledgements

Author contributions

G.G., V.K. and E.S. proposed the transmissive monochromator scheme and the double-chicane setup. W.D., C.G., G.G., M.G., V.K., C.L., S.L., T.L., E.S., H.S., L.S., S.S. and S. Tomin developed the software, control-room scripts/graphical user interfaces and simulations for the design and commissioning phases. D.S., J.A. and S. Kearney designed the monochromator chamber. V.B., L.S. and S. Terentiev produced and mounted the crystals on the holders. X.D., S. Karabekyan, D.L.C., M.V., T.W. and M.Y. engineered and installed the HXRSS system and related diagnostics. F.B., G.G., M.G., S. Karabekyan, N.K., D.L.C., S.L., T.M., L.S., H.S., M.S., A.R.-F., S.S., V.S., T. Tanikawa, S. Terentiev, S. Tomin and M.Y. commissioned the HXRSS system. G.G., S.L., M.G. and S.S. designed the experiments discussed in this Article. S.L., C.G., G.G. M.G., S. Karabekyan, V.K., N.K., C.L., T.L., N.M., W.Q., S.S., S. Tomin and J.Y. tuned the HXRSS setup and took data during the experiments. U.B., Y.C., C.G., G.G., M.G., V.K., N.K., S. Karabekyan, C.L., J.Y., S.L., A.M., N.M., T.M., W.Q., L.S., H.S., M.S., S.S., V.S., S. Tomin, T. Tanikawa, A.T. and M.Y. conducted the experiments. C.L., S.L., T.L., V.S., S.S. and J.Y. analysed the data. S.A., W.D., S. Karabekyan, T. Tschentscher, T.W. and M.Y. supported the operations during commissioning and experiments. W.D. and H.S. managed the project. A.M., G.G., C.L., S.L., T.L., T. Tschentscher and J.Y. wrote the manuscript with input from all co-authors.

Funding

Competing interests

The authors declare no competing interests.

Additional information

Supplementary information The online version contains supplementary material available at https://doi.org/10.1038/s41566-023-01305-x.

Correspondence and requests for materials should be addressed to Gianluca Geloni.

Peer review information *Nature Photonics* thanks Zhirong Huang, Heung-Sik Kang and Makina Yabashi for their contribution to the peer review of this work.

Reprints and permissions information is available at www.nature.com/reprints.